energies

MDPI

Article

Pelican Optimization Algorithm-Based Proportional–Integral–Derivative Controller for Superior Frequency Regulation in Interconnected Multi-Area Power Generating System

Abidur Rahman Sagor [1], Md Abu Talha [1], Shameem Ahmad [1,*], Tofael Ahmed [2], Mohammad Rafiqul Alam [2], Md. Rifat Hazari [1] and G. M. Shafiullah [3,*]

[1] Department of Electrical and Electronic Engineering, Faculty of Engineering, American International University–Bangladesh, Dhaka 1229, Bangladesh; abidsagor83@gmail.com (A.R.S.); abutalha8324@gmail.com (M.A.T.); rifat@aiub.edu (M.R.H.)
[2] Department of Electrical and Electronic Engineering, Chittagong University of Engineering & Technology, Chattogram 4349, Bangladesh; tofael@cuet.ac.bd (T.A.); mraeee@cuet.ac.bd (M.R.A.)
[3] School of Engineering and Energy, College of Science, Technology, Engineering and Mathematics, Murdoch University, Perth, WA 6150, Australia
* Correspondence: ahmad.shameem@aiub.edu (S.A.); gm.shafiullah@murdoch.edu.au (G.M.S.)

Abstract: The primary goal of enhancing automatic generation control (AGC) in interconnected multi-area power systems is to ensure high-quality power generation and reliable distribution during emergencies. These systems still struggle with consistent stability and effective response under dynamic load conditions despite technological advancements. This research introduces a secondary controller designed for load frequency control (LFC) to maintain stability during unexpected load changes by optimally tuning the parameters of a Proportional–Integral–Derivative (PID) controller using pelican optimization algorithm (POA). An interconnected power system for ith multi-area is modeled in this study; meanwhile, for determining the optimal PID gain settings, a four-area interconnected power system is developed consisting of thermal, reheat thermal, hydroelectric, and gas turbine units based on the ith area model. A sensitivity analysis was conducted to validate the proposed controller's robustness under different load conditions (1%, 2%, and 10% step load perturbation) and adjusting nominal parameters (R, T_p, and T_{ij}) within a range of ±25% and ±50%. The performance response indicates that the POA-optimized PID controller achieves superior performance in frequency stabilization and oscillation reduction, with the lowest integral time absolute error (ITAE) value showing improvements of 7.01%, 7.31%, 45.97%, and 50.57% over gray wolf optimization (GWO), Moth Flame Optimization Algorithm (MFOA), Particle Swarm Optimization (PSO), and Harris Hawks Optimization (HHO), respectively.

Keywords: automatic generation control; pelican optimization; PID; load frequency control; integral time absolute error; interconnected power systems

check for updates

Citation: Sagor, A.R.; Talha, M.A.; Ahmad, S.; Ahmed, T.; Alam, M.R.; Hazari, M.R.; Shafiullah, G.M. Pelican Optimization Algorithm-Based Proportional–Integral–Derivative Controller for Superior Frequency Regulation in Interconnected Multi-Area Power Generating System. *Energies* **2024**, *17*, 3308. https://doi.org/10.3390/en17133308

Academic Editor: Oscar Duque-Perez

Received: 22 May 2024
Revised: 22 June 2024
Accepted: 27 June 2024
Published: 5 July 2024

Copyright: © 2024 by the authors. Licensee MDPI, Basel, Switzerland. This article is an open access article distributed under the terms and conditions of the Creative Commons Attribution (CC BY) license (https://creativecommons.org/licenses/by/4.0/).

1. Introduction

The growing importance of electricity generation and environmental sustainability necessitates robust, efficient, and resilient electrical power systems. The North American Blackout of 2003 [1] highlighted the importance of distributed control in large-scale interconnected power systems, with a specific focus on the ability to withstand physical and network communication challenges as well as the ability to recover and reorganize autonomously. The European interconnected grid also exemplifies how interconnected power systems can meet these challenges by facilitating efficient distribution and sharing of electrical power [2]. Moreover, these interconnected grids achieve energy security and sustainability by balancing loads and integrating renewable energy sources to satisfy increasing energy demands. This dual approach benefits all stakeholders and improves

power reliability for residents, ensuring reliable energy supply, enhancing environmental protection, and enabling energy trade and communication between nations [3].

In connection with the operation and control of power systems, providing a sufficient reliable supply of high-quality electricity with high standards is a priority. Achieving this target depends critically on load frequency control (LFC). There are several control areas in an interconnected power system where all generators constitute a cohesive unit [4]. During steady-state operation, variations in load demand lead to changes in kinetic energy stored within generator prime movers. Consequently, these changes affect speed and frequency. Hence, effective control of load frequency becomes indispensable for the secure operation of the power system [5–10]. LFC is a technique that adjusts the power output of controlled generators in a particular area in response to fluctuations in system frequency, tie-line, or their interaction. The goal is to maintain the scheduled system frequency and establish interchange with additional areas within predetermined limits [11–14]. An optimal control method that ensures frequency stability and the intended tie-line power flow as well as zero steady-state error and accidental interchange is sought. The conventional Proportional–Integral (PI) controller stands out as the most widely used among the array of load frequency controllers available [15,16]. Recent advancements in control strategies for power systems have focused on predictive control methods and reinforcement learning techniques to enhance system performance and stability. For instance, learning-based predictive control can improve the dynamic response and robustness of power converters [17,18] and voltage source inverters [19] in a power system. However, their effectiveness diminishes as system complexity increases due to load fluctuations and boiler dynamics [20]. Hence, there is a need for controllers capable of addressing these challenges. Artificial intelligence (AI) controllers, such as the Neural Network Control approach, prove more fitting in this context [21]. These techniques possess the advantage of providing model-free control descriptions, eliminating the need for model identification. Employing an Advanced Adaptive Control setup like the ANN controller is particularly beneficial, as it offers swifter control than other methods [22]. To enhance the performance of conventional controllers (PI and PID) and neural controllers, a proposal is made for an Artificial Neural Network (ANN) controller within a two-area interconnected hydro–thermal and thermal–thermal power plant scenario. Including a neural controller sliding surface is motivated by variable structure control (VSC). This concept involves utilizing a sliding surface that leads to robust control systems, often resulting in invariant systems. Invariance implies that the system remains unaffected mainly by parametric uncertainty and external disturbances [23,24]. However, traditional PID algorithms offer simplicity, reliability, low computational demands, fast response, less expensive, and ease of practical implementation and tuning, making them superior to AI controllers in straightforward, well-defined control systems [25–27].

The investigation of an LFC conflict in a nonlinear power generation network is conducted by implementing an innovative hybrid GSA-tuned optimized controller [28]. A PSO-PID controller and a PID controller based on the flower pollination algorithm (FPA) were developed to analyze the frequency regulation of nuclear power facilities integrated with networks of thermal, gas, hydro, and PV power systems to address LFC conflicts [29]. These techniques provide premature convergence and do not convert the global optima; also, early convergence becomes caught in local optima when used for complex problems. The GWO algorithm was employed in [30,31] to modify the controller parameters. The simulation results demonstrated that the GWO algorithm could rapidly suppress the power system frequency and power oscillations. However, as the algorithm progresses, the lead wolf's weight increases unsustainably, making it simple to enter the local optimum. The gray wolf algorithm was employed in [32,33] to optimize and regulate the frequency of multi-area loads. At the same time, it encountered the convergence issue. In a later phase, the proportion of the lead wolf grew excessively high, resulting in local optima. The gray wolf optimization algorithm was implemented in [34] to optimize the time-delayed load frequency control problem. The gray wolf algorithm with fixed weight demonstrated a

more favorable outcome in the domain of optimal frequency control [35]. The method cannot exist for local search due to slow convergence speed at the later part of the iteration; however, it resulted in slow convergence and poor precision and accuracy.

Stabilizing load frequency in interconnected power systems is a research area that has seen various algorithms proposed to enhance the performance of Proportional–Integral–Derivative (PID) controllers. El-Hameed and El-Fergany [36] pioneered the integration of the Water Cycle Algorithm (WCA) with PID controllers, addressing nonlinearity in interconnected power systems. This approach exhibits delayed convergence and limited exploration and exploitation. The technique demonstrates a frequency response that requires more time to settle. Guha et al. [37] advanced this domain by implementing the Backtracking Search Algorithm (BSA) in the LFC of a multi-area interconnected power system, demonstrating improved system stability and robustness. BSA generally exhibits a slow convergence rate during its early stages due to its disregard for the significance of the optimal individual, which challenges its ability to attain a satisfactory outcome. This is the reason the frequency response requires more time to settle down. Yeboah et al. [38] employed the Gravitational Search Algorithm (GSA) to address LFC challenges in multi-area power systems, offering a novel approach to system optimization by mimicking the law of gravity and mass interactions. GSA suffers from premature convergence due to rapid reduction in diversity. Frequency response requires more time to settle down. Comparative studies by Hakimuddin et al. [39] explored the efficacy of Genetic Algorithms (GAs), Bacteria Foraging Algorithms (BFAs), Particle Swarm Optimization (PSO) [40], and Mayfly Algorithm (MA) [41] in multi-source power plants, highlighting the competitive nature of these algorithms and also highlighting the need for more comprehensive comparative frameworks. This technique converges quickly, gets stuck in the local optimal solution, and takes more time to settle. Mohanty et al. [42] introduced the Moth Flame Optimization Algorithm (MFOA), demonstrating the potential of bio-inspired algorithms in achieving fine-tuned control over LFC in power systems. This technique provides limited population variety and falls into local optima and premature convergence. The outcomes were less time-settled than other techniques, but overall performance was low. Acharyulu et al. [43] and Jagatheesan et al. [44] proposed using Green Anaconda Optimization and gray wolf optimization algorithms, focusing on renewable energy and diverse power generation systems. These techniques are frequency response, and more time is required for stability. However, in this research, paperwork is a benchmark for the proposed pelican optimization algorithm (POA)-PID controller, aiming to further reduce frequency deviations and the cost function ITAE in a complex four-area power system. The proposed POA technique outperforms existing techniques by effectively balancing exploration and exploitation, achieving superior and more competitive performance [45–47]. It classifies a population-based approach that converges to a nearly optimal solution through an iterative procedure. The proposed technique, LFC, rapidly resolved the issue of time to settle.

The above comprehensive literature review underscores the extensive exploration of various optimization algorithms to fine-tune auxiliary controller gains for implementing LFC in multi-area interconnected power systems. In this paper, the POA is proposed for optimizing the gain values of PID controllers under a 1% step load perturbation across a mixed thermal–hydro–gas turbine power plant. Given the prevalence of thermal power generation due to its scalability and accessibility, its environmental impact remains a significant drawback. This study aims to mitigate such drawbacks by integrating conventional thermal, reheat thermal power plants, gas turbine power plants, and hydropower plants, enhancing the power generation mix's efficiency and sustainability. The effectiveness of the newly optimized regulation technique is assessed by comparing it against the performance metrics of PID controllers tuned via gray wolf optimization (GWO), Harris Hawks Optimization (HHO), Particle Swarm Optimization (PSO), and Moth Flame Optimization Algorithm (MFOA). Additionally, the robustness and adaptability of the proposed POA-PID controller are evaluated under varying load disturbances, and parameter changes $\pm 25\%$ and $\pm 50\%$ of

their nominal values, highlighting its superior performance and efficiency in maintaining system stability and operational efficiency.

The main contributions of this paper are as follows:

- Interconnected power systems with and without pollution-free generating sources are modeled for ith area. Further, based on the modeled ith area power systems network, a four-area power network is developed for testing and validation purposes.
- Introduced a secondary controller for LFC that utilizes POA-based PID controller tuning parameters to maintain stability during unexpected load changes.
- Conducted comprehensive robustness analysis under varying load conditions and variations in parameters, confirming the effectiveness of the POA-PID controller.
- Proposed POA-based optimization technique performance is compared against established methods like GWO, PSO, MFOA, and HHO to set new benchmarks for load frequency and tie-line power flow control efficiency, showing significant improvements in ITAE and system stability.

The article is arranged as follows: Section 2 is the mathematical modeling of the proposed four-area interconnected power system. Section 3 shows the structure of the controller and optimization technique. Section 4 shows the analysis investigated between the proposed controller POA-PID and other algorithms, including GWO, MFOA, PSO, and HHO-PID controller. Finally, the conclusion about optimization techniques is in Section 5.

2. Modeling of the Power System

A multi-area interconnected power system was used for the LFC study. Thermal plants comprise Area 1 of the multi-area power system, followed by thermal plants with reheat in Area 2, hydropower plants in Area 3, and gas turbine plants in Area 4, as depicted in Figure 1. A tie-line connecting every location in an interconnected system is the fundamental structure for electricity exchange. Any nearby areas will experience an increase in generation, a modification in connection line power, and a reduction in frequency when there is a power change in one area. Nevertheless, should the power system function normally, the demand of each area will be fulfilled at a consistent frequency, and each region will autonomously adjust to variations in load. Each specific area contributes to eliminating area control error (ACE), which is present in every area.

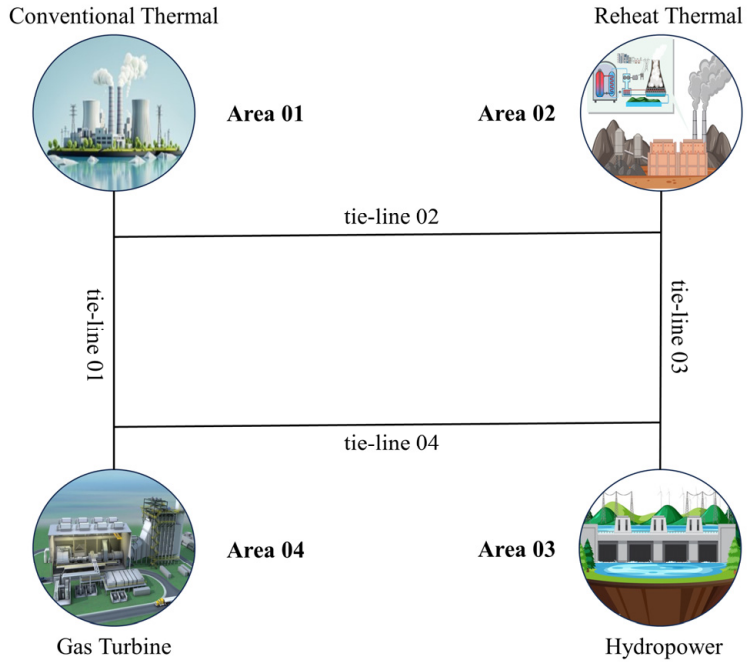


Figure 1. Multi-area interconnected power system.

2.1. Mathematical Modeling for ith Interconnected Power Systems

In recent years, power systems have been integrated into N number of control areas interconnected by tie-lines, as seen in Figure 2 for the *i*th power systems. The *i*th systems can be written as [34]

$$\Delta\dot{X}_{Gi}(t) = \frac{1}{T_{Gi}}(\Delta P_{ci}(t) - \frac{1}{R_i}\Delta f_i(t) - \Delta X_{gi}(t) - \Delta E_i(t)) \quad (1)$$

$$\Delta\dot{P}_{Gi}(t) = \frac{1}{T_{ti}}(\Delta X_{gi}(t) - \Delta P_{Gi}(t) \quad (2)$$

$$\Delta\dot{f}_i(t) = \frac{K_{Pi}}{T_{Pi}}(\Delta P_{Gi}(t) - \Delta P_{Li}(t) - \Delta P_{tiei}(t) - \frac{1}{K_{Pi}}\Delta f_i(t)) \quad (3)$$

$$\Delta\dot{P}_{tiei}(t) = 2\pi\textstyle\sum_{j=1,j\neq1}^{N} T_{ij}(\Delta f_i(t) - \Delta f_j(t)) \quad (4)$$

$$ACE_i(t) = \Delta P_{tiei}(t) + \beta_i\Delta f_i(t) \quad (5)$$

Here,

$$x_i(t) = \left[\Delta X_{gi}(t)\Delta P_{Gi}(t)\Delta f_i(t)\Delta P_{tiei}(t)\right]^T;\ y_i(t) = ACE_i(t);\ \text{and}\ u_i(t) = \Delta P_{ci}(t)$$

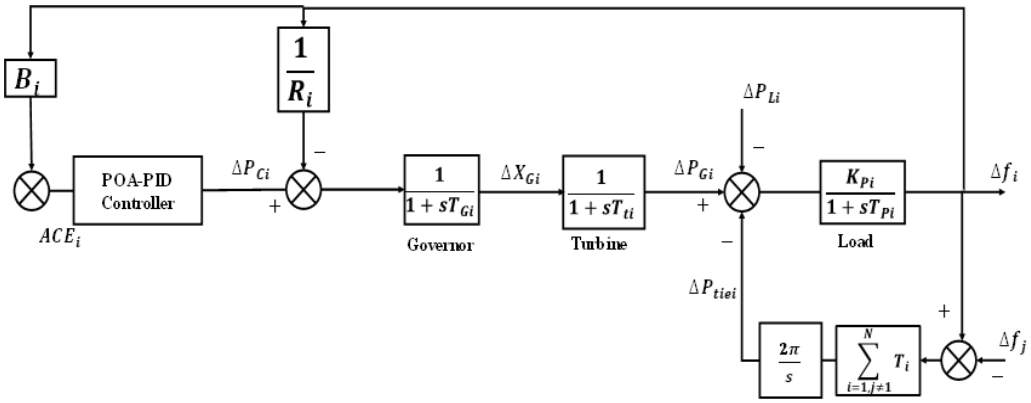


Figure 2. Block diagram of ith interconnected power systems.

From the above equation, the system has

$$\dot{x}_i(t) = A_i x_i(t) + B_i u_i(t) + D_i\Delta P_{Li}(t) + \sum_{j=1,j\neq1}^{N} F_{ij}x_j(t) \quad (6)$$

$$\dot{y}_i(t) = C_i x_i(t) \quad (7)$$

where

$$A_i = \begin{bmatrix} \frac{1}{T_{Gi}} & 0 & -\frac{1}{R_i.G_i} & 0 \\ \frac{1}{T_{ti}} & -\frac{1}{T_{ti}} & 0 & 0 \\ 0 & \frac{K_{Pi}}{T_{Pi}} & -\frac{1}{T_{ti}} & -\frac{K_{Pi}}{T_{Pi}} \\ 0 & 0 & 2\pi\sum_{j=1,j\neq1}^{N} F_{ij} & 0 \end{bmatrix};$$

$$B_i = \begin{bmatrix} \frac{1}{T_{Gi}} \\ 0 \\ 0 \\ 0 \end{bmatrix};\ D_i = \begin{bmatrix} 0 \\ 0 \\ -\frac{K_{Pi}}{T_{Pi}} \\ 0 \end{bmatrix};\ F_{ij} = \begin{bmatrix} 0 & 0 & 0 & 0 \\ 0 & 0 & 0 & 0 \\ 0 & 0 & 0 & 0 \\ 0 & 0 & -2\pi T_{ij} & 0 \end{bmatrix};$$

$$\text{and } C_i = \begin{bmatrix} 0 & 0 & \beta_1 & 1 \end{bmatrix}.$$

2.2. Mathematical Modeling for the Proposed Power System

As discussed in [48,49], the mathematical expression of the proposed four-area power system is

2.2.1. Thermal Power System without and with Reheat

Combining the blocks makes it simple to obtain a complete block diagram of an isolated power system consisting of a turbine, generator, governor, and load. Figure 3 depicts a complete block diagram of a thermal plant without reheat, and Figure 4 depicts a thermal plant with reheat.

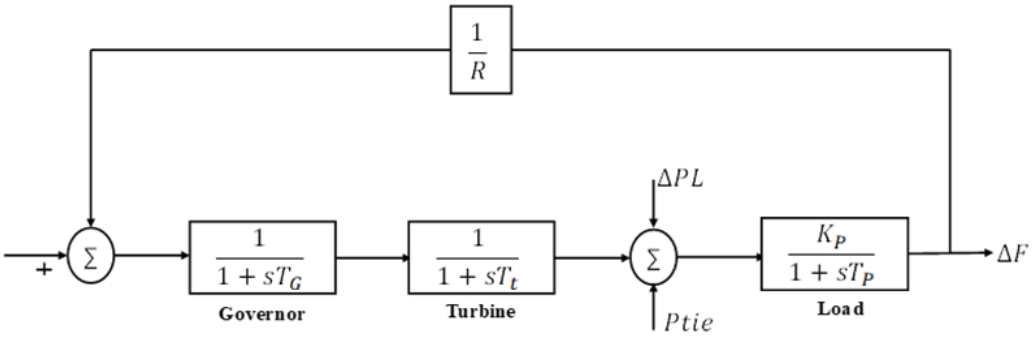


Figure 3. Block diagram of thermal power system without reheat.

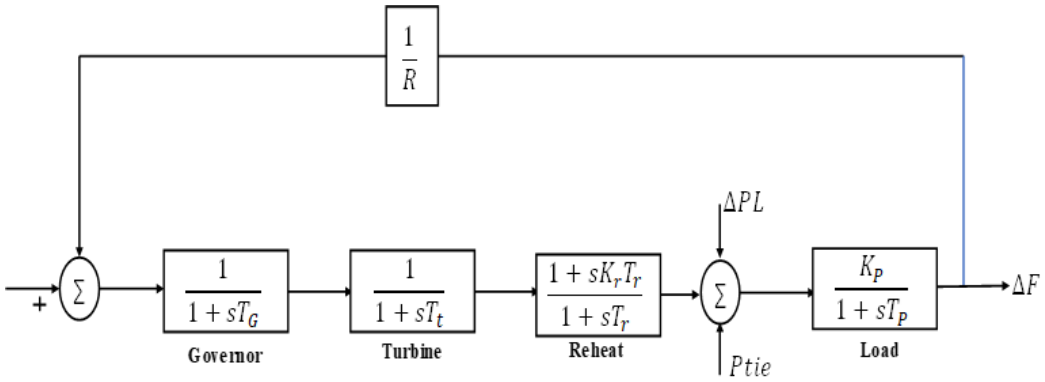


Figure 4. Block diagram of thermal power system with reheat.

Modeling of thermal power system:

$$\text{Governor} = G = \frac{1}{1+sT_{sg}} \tag{8}$$

$$\text{Steam turbine} = S_t = \frac{1}{1+sT_t} \tag{9}$$

$$\text{Reheater} = \frac{1+sK_rT_r}{1+sT_r} \tag{10}$$

2.2.2. Hydropower System

Hydropower resources operate using a method similar to that of thermal plants. The input of the hydro turbine is water, not steam. It is essential to make adjustments for the initial droop characteristics that arise from the reduced pressure of the turbine when the gate valve is opened. Hydro turbines exhibit irregular responses due to the inertia of water; a modification in valve position induces an initial turbine power change that contrasts the design requirement. To achieve consistent control performance, a substantial transient droop that includes an extended period of resettling is required, as depicted in Figure 5. The compensation constrains the movement of the valve until the water flow

power output reaches a level. As a result, the governor exhibits excessive droop during fast speed variations but minimal droop during steady state [50].

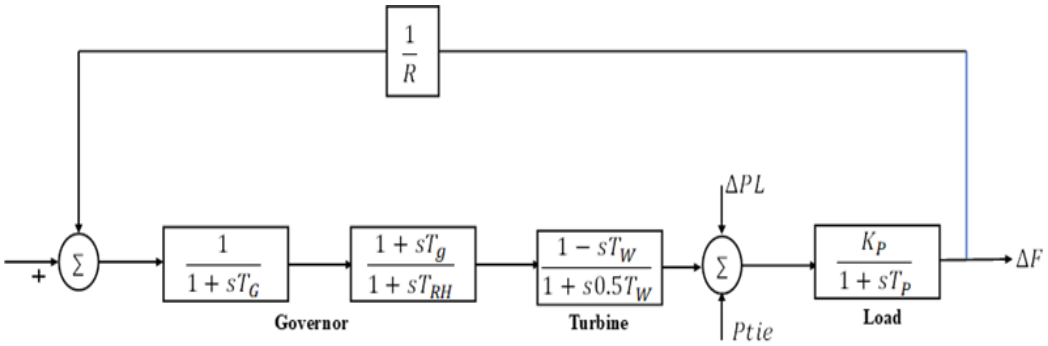


Figure 5. Block diagram of hydropower system.

Modeling of hydropower system:

$$\text{Governor} = \frac{1}{1+sT_{gh}} \tag{11}$$

$$\text{Drop Compensation} = \frac{1+sT_g}{1+sT_{RH}} \tag{12}$$

$$\text{Penstock turbine} = \frac{1+sT_w}{1+s0.5T_w} \tag{13}$$

2.2.3. Gas Turbine Power System

Gas turbine power plants generally comprise the following elements: the gas turbine, combustor, fuel system, speed governor, and valve positioning. The load frequency model of the gas turbine structure is shown in Figure 6.

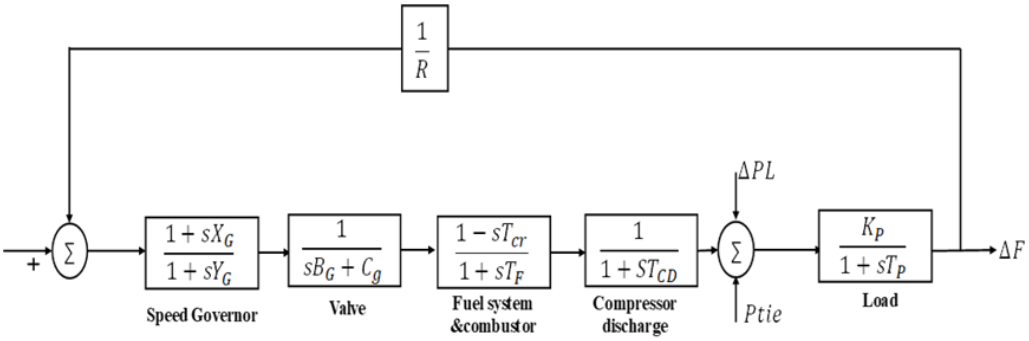


Figure 6. Block diagram of gas turbine power system.

Modeling of gas power system:

$$\text{Valve positioner} = \frac{1}{sB_g+C_g} \tag{14}$$

$$\text{Speed Governor} = \frac{sX_g+1}{sY_g+1} \tag{15}$$

$$\text{Combustion reaction} = \frac{-sT_{cr}+1}{sT_F+1} \tag{16}$$

$$\text{Compressor discharge} = \frac{1}{sT_{CD}+1} \tag{17}$$

The governor, reheater, and steam turbine time constant are denoted by the symbols T_{sg}, T_r, and T_t, respectively. In that order, the time constants for the hydropower plant, governor, drop compensation, and penstock turbine are T_{gh}, T_r, T_{rh}, and T_w, respectively. The gas turbine constants for the positioner and the gas turbine valve are denoted as B_g and

C_g, respectively. The governor's lead and lag time constants are represented by X_g and Y_g, respectively. T_f represents the time constant for fuel, T_{cr} represents the time delay for the combustion reaction, and T_{CD} represents the time constant for compressor discharge volume.

Tie-line power flow among four area power systems as shown in Figure 1 can be written as

$$P_{12} = \frac{|E_1||E_2|}{X_{12}} sin\delta_{12} \tag{18}$$

$$P_{23} = \frac{|E_2||E_3|}{X_{23}} sin\delta_{23} \tag{19}$$

$$P_{34} = \frac{|E_3||E_4|}{X_{34}} sin\delta_{34} \tag{20}$$

$$P_{14} = \frac{|E_1||E_4|}{X_{14}} sin\delta_{14} \tag{21}$$

In addition, the expression for tie-line power deviation among four area power systems is

$$\sum_{j=1}^{N} \Delta P_{tie\ ij} = \sum_{j=1}^{N} T_{ij}\Delta\delta_i - \sum_{j=1}^{N} T_{ij}\Delta\delta_j \tag{22}$$

These are the Laplace transforms of Equations (18)–(21):

$$\Delta P_{tie\ ij} = \sum_{j=1}^{N} \Delta P_{tie\ ij} = \frac{2\pi}{s}[\sum_{j=1}^{N} T_{ij}\Delta f_i\ - \sum_{j=1}^{N} T_{ij}\Delta f_j\ ] \tag{23}$$

In the given context, the slope of the power angle curve at the initial operating angle (120°/phase) is denoted as T_{ij}, and P_{ri} is rated capacity of each area.

$$T_{ij} = \frac{|E_i||E_j|}{P_{ri}X_{ij}} cos\delta \tag{24}$$

$$\sum_{j=1}^{N} \alpha_{ij} = -\sum_{j=1}^{N} \frac{P_{ri}}{P_{rj}} \tag{25}$$

$$\sum_{j=1}^{N} \Delta P_{ji} = \sum_{j=1}^{N} \alpha_{ij}\Delta P_{ij} \tag{26}$$

When four areas are interconnected via a transmission line, the variation in mechanical power for each area is

$$\Delta P_{mi} = \frac{-\Delta\omega}{R_i} \qquad \text{for } i = 1, 2, \ldots\ldots\ldots, N \tag{27}$$

Characteristics of the frequency response (β) for each area are

$$\beta_i = D_i + \frac{1}{R_i} \qquad \text{for } i = 1, 2, \ldots\ldots\ldots, N \tag{28}$$

Consequently, the frequency deviation for load variation in each area is

$$\Delta\omega_i = \frac{\Delta P_{Li}}{\sum_{j=1}^{N} \beta_j} \qquad \text{for } i = 1, 2, \ldots\ldots\ldots, N \tag{29}$$

Lastly, the area control error (ACE) for the ith area in this power system is a metric used to maintain the balance between electricity supply and demand across regions. It combines the deviation in power flow across interconnected multi-area tie-lines (ΔP_{tie}) and the deviation in the area's frequency ($\Delta\omega_i$), adjusted by a frequency bias factor (β_i).

The ACE indicates how much the actual conditions have deviated from the scheduled conditions, guiding operators on whether to increase or decrease generation or load to stabilize the power system.

$$ACE_i = \Delta P_{tie} + \beta_i \Delta\omega_i \qquad \text{for } i = 1, 2, \ldots\ldots\ldots, N \tag{30}$$

2.3. Proposed Four-Area Power System

The study focuses on improving frequency regulation in multi-area power systems by developing a comprehensive Simulink model within the MATLAB/Simulink environment. Figure 7 represents a four-area power network with distinct power generation units, each parameterized with nominal system values from [48,49], shown in Appendix A. A 1% step load perturbation was introduced to simulate realistic operational stress. The model includes nominal values such as governor time constants (0.08 s for thermal and 5.0 s for hydro), turbine time constants (0.3 s for thermal and 28.75 s for hydro's transient droop), reheat and water time constants, and various constants for gas turbines. Each area has a rated capacity of 2000 MW, harmonized by a 60 Hz frequency standard, and a system inertia constant at 5 MWs/MVA. The interconnecting tie-lines, defined by a frequency bias and power system time constant, are crucial for maintaining system stability amidst dynamic load conditions. The Simulink model is a vital instrument in the investigation, providing a simulated environment to assess and optimize LFC across the interconnected four-area power systems.

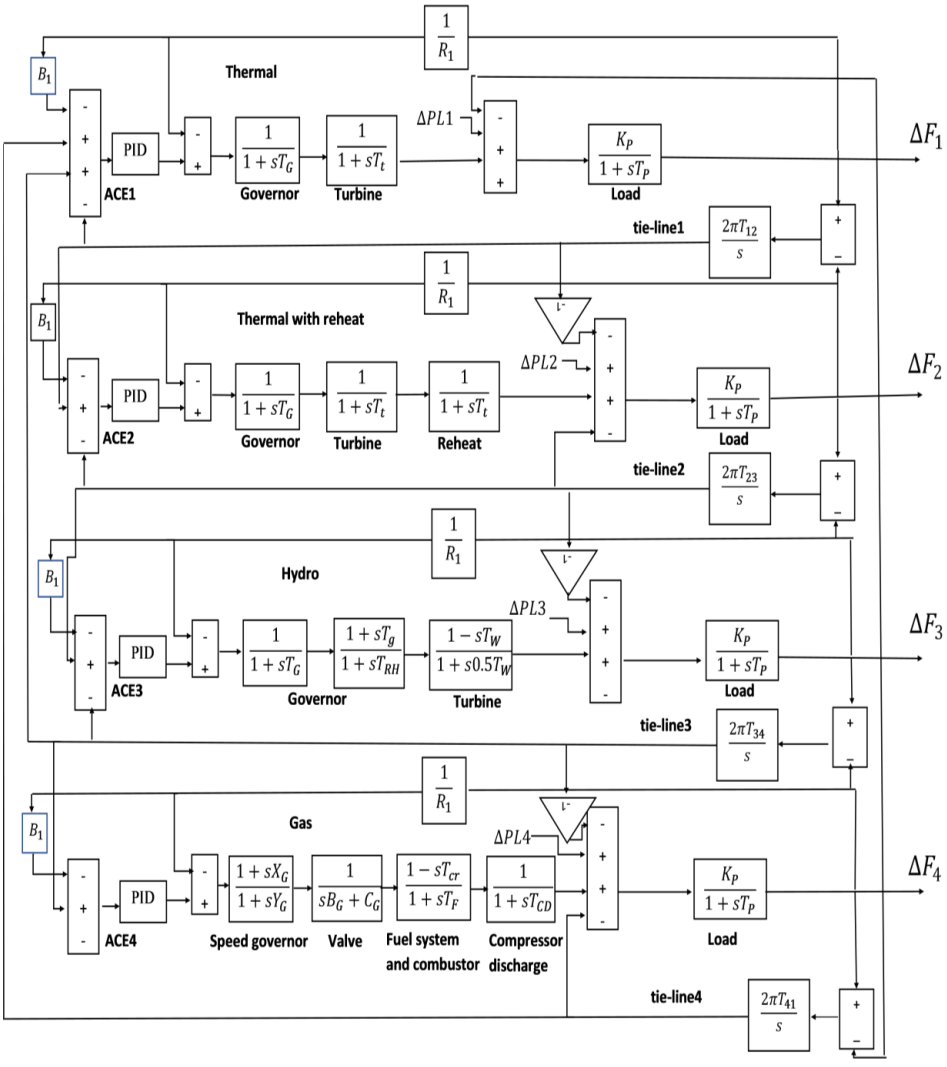


Figure 7. Mathematical model of the proposed four-area power system.

3. Structure of the PID Controller and Optimization Technique

3.1. PID Controller

The proposed PID controller is crucial for the regulation of system frequency and tie-line power flow deviations during step load perturbation conditions by reducing the settling time in deviation. PID controllers that are employed by researchers are the most frequently employed in various sectors. PID controllers are defined by three control actions: the derived control action, integral control action, and proportional control action. The transfer function of the PID controller is illustrated in Equation (31). The controller improves the efficacy and stability in response to fast-settled responses [51,52].

$$G_{PID} = K_p + \frac{K_i}{s} + K_d s \tag{31}$$

The proportional, integral, and derivative gain values are denoted by K_p, K_i, and K_d, respectively. The controller's performance is assessed independently of these three criteria. The controller's gain value is maximized by employing the standard tuning procedure; however, optimization of the controller's gain and response necessitates additional time and results in inadequate time domain specification parameter values. The PID controller gain value is optimized in this study by employing the ITAE cost function and utilizing the pelican optimization algorithm (POA) technique, thereby overcoming this disadvantage [51,53]. The cost function of ITAE is illustrated below:

$$J_{ITAE} = \int t.\,|ACE|dt \tag{32}$$

3.2. Pelican Optimization Algorithm (POA)

POA, a novel algorithm inspired by nature, was developed in 2022 by Trojovský et al. [44]. The POA method is population-based; pelicans comprise this population. In algorithms based on populations, each element signifies a prospective solution. Based on their position in the search space, each member of the population proposes values for the variables associated with the optimization problem. First, the population members are randomly distributed using Equation (33), which is constrained by the upper and lower bounds of the issue [41].

$$X_{i,j} = l_j + rand.\left(u_j - l_j\right),\ i = 1, 2, \ldots, N,\ j = 1, 2, \ldots,\ m, \tag{33}$$

The value of the jth variable is determined by deducing it from the ith feasible solution, denoted as $X_{i,j}$. The population is N. There are rm issue variables. $rand$ is a random number that is between 0 and 1. The jth lower limit of the problem variables is l_j, and their jth upper bound is u_j.

$$X = \begin{bmatrix} X_1 \\ \vdots \\ X_i \\ \vdots \\ X_N \end{bmatrix}_{N\times m} = \begin{bmatrix} x_{1,1} & \cdots & x_{1,j} & \cdots & x_{1,m} \\ \vdots & \ddots & \vdots & \iddots & \vdots \\ x_{i,1} & \cdots & x_{i,j} & \cdots & x_{i,m} \\ \vdots & \iddots & \vdots & \ddots & \vdots \\ x_{N,1} & \cdots & x_{N,j} & \cdots & x_{N,m} \end{bmatrix}_{N\times m} \tag{34}$$

where X is the matrix that represents the pelican population, and X_i represents the ith individual pelican. As every individual of the POA population is a pelican, this may present an acceptable resolution. Thus, evaluating the problem's objective function is feasible by analyzing every possible solution. Equation (35) and a vector referred to as the objective function vector are utilized to ascertain the values of the objective function.

$$F = \begin{bmatrix} F_1 \\ \vdots \\ F_i \\ \vdots \\ F_N \end{bmatrix}_{N\times 1} = \begin{bmatrix} F(X_1) \\ \vdots \\ F(X_i) \\ \vdots \\ F(X_N) \end{bmatrix}_{N\times 1} \quad (35)$$

The pelican's hunting process consists of two distinct phases, which are referred to as exploitation and exploration. Exploration entails movement in the direction of the prey, as opposed to exploitation, which requires flying on the water's surface. During the initial phase, pelicans locate and approach their prey. The exploration performance of POA is enhanced due to the random generation of the prey's position. The first phase is mathematically represented by Equation (36).

$$x_{i,j}^{P_1} = \begin{cases} x_{i,j} + rand.(p_j - l.x_{i,j}), & F_p^1 < F_i; \\ x_{i,j} + rand.(x_{i,j} - p_j), & else, \end{cases} \quad (36)$$

where F_p and $x_{i,j}^{P_1}$ represent the prey objective function value, a random number l equal to one or two, and the ith pelican's new status in the jth dimension based on the first phase. A new position of a pelican becomes permissible within the bounds of POA if the objective function value increases at that particular location. By employing this methodology, known as "effective updating", the algorithm avoids its progression through suboptimal regions. From a mathematical standpoint,

$$X_i = \begin{cases} X_i^{P_1}, & F_i^{P_1} < F_i; \\ X_i, & else, \end{cases} \quad (37)$$

where $X_i^{P_1}$ represents the updated status of the ith pelican, whereas $F_i^{P_1}$ represents the value of the pelican's objective function calculated during the initial phase. During the second phase, pelicans employ the water's surface to generate upward propulsion for the fish by extending their wings, subsequently trapping the prey in their throat bag. Consequently, pelicans can catch a greater quantity of fish. The exploitation potential of POA is enhanced during this phase as the algorithm approaches more optimal solutions in the hunting zone. The hunting procedure is formulated as follows:

$$x_{i,j}^{P_2} = x_{i,j} + R.\left(1 - \frac{t}{T}\right).(2.rand - 1).x_{i,j} \quad (38)$$

where $x_{i,j}^{P_2}$ denotes the updated state of the ith pelicans in the jth dimension during the second phase. The constant R equals 0.2 and $R.(1 - t/T)$. is an expression using t and T variables. The neighborhood radius of $x_{i,j}$ is determined by the iteration counter t and the maximum number of iterations T. At this point, the approval or rejection of the newest pelican position has been determined through efficient updating, as illustrated in Equation (39):

$$X_i = \begin{cases} X_i^{P_2}, & F_i^{P_2} < F_i; \\ X_i, & else, \end{cases} \quad (39)$$

where represents the new status of the $X_i^{P_2}$ is the i^{th} pelican and denotes the objective function value of the pelican. This next iteration begins once every member of the population has been updated. A series of operations guided by Equations (36)–(39) are repeated throughout this process until the execution is finished.

3.3. The Optimization Flow of the Proposed PID Controller

The POA is a novel optimization technique that uses the foraging behavior of pelicans to optimize PID controller parameters within a power system network. The POA initializes

a population of candidate solutions, representing pelicans, each corresponding to a potential set of PID controller parameters. The size of this population (N) and the number of iterations (T) are predetermined parameters that influence the scope and depth of the search process.

The process iterates through two distinct phases. The first phase, 'Moving towards prey', simulates the pelican's exploratory behavior as it searches for prey. Each solution is updated by stochastically adjusting its position in the search space, guided by Equation (35), which encapsulates an element of randomness akin to the unpredictable nature of prey movement. The updated positions are evaluated using the objective function, which measures the quality of the solution in terms of system performance.

The second phase, 'Winging on the water surface', shifts to an exploitation strategy, reflecting the pelican's action of floating and waiting on the water surface for the optimal moment to catch prey. The iterative process continues until the termination condition is met, typically defined by reaching the maximum number of iterations (T).

The output of the POA is the best candidate solution, which corresponds to the optimized PID controller parameters that minimize the objective function, typically a measure of system performance. With its dual-phase strategy, the POA technique mirrors pelicans' adaptive foraging patterns, making it effective in complex, multimodal optimization landscapes commonly found in power system control problems. The flowchart in Figure 8 and the pseudocode in Figure 9 provide a clear algorithmic structure for implementation, ensuring efficient and effective solutions.

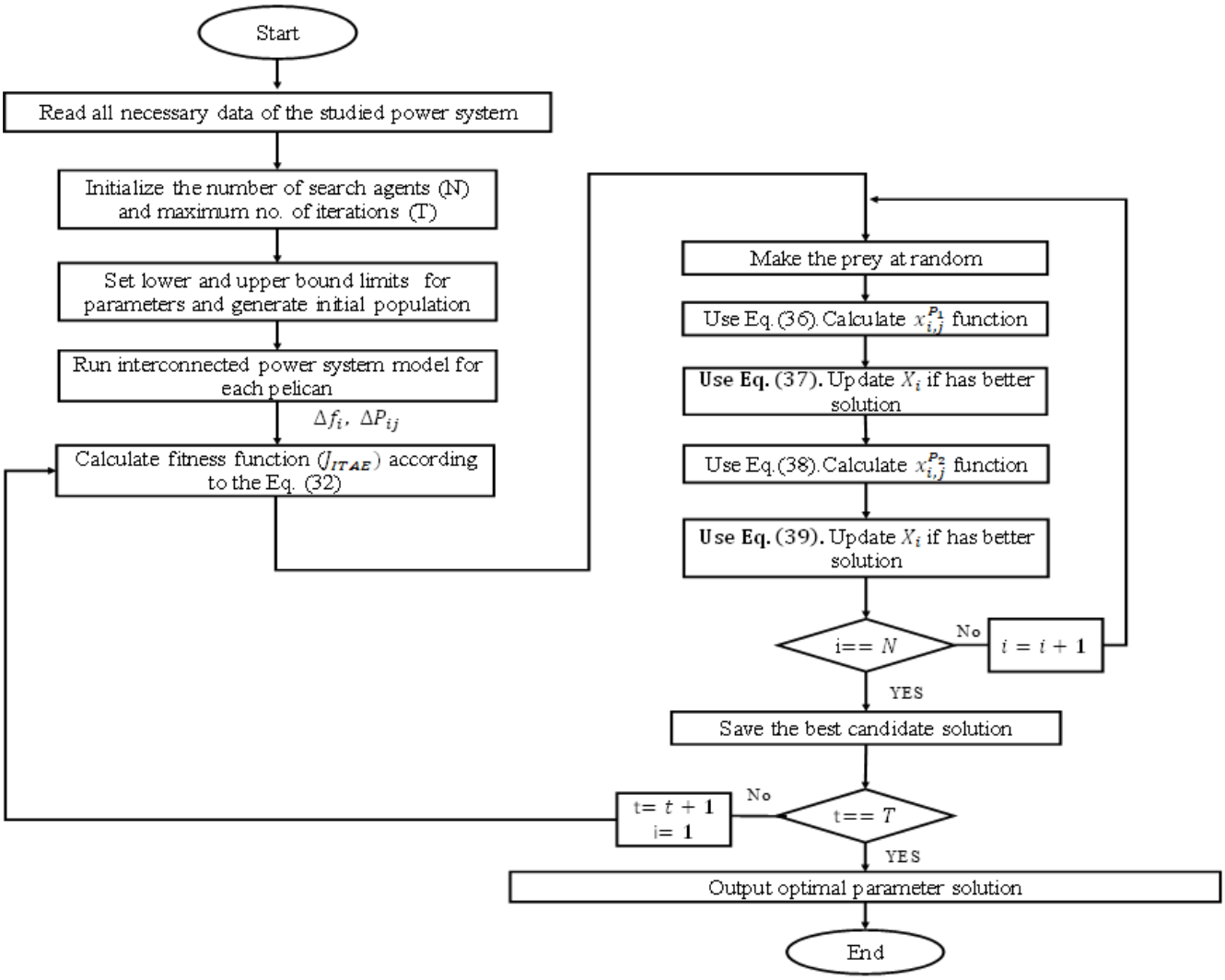


Figure 8. POA technique-based PID controller optimization flowchart.

```
Input the optimization problem information
Determine the POA population size (N) and the number of iterations (T)
Initialization of the position of pelicans and calculate the objective function
For t = 1:T
    Generate the position of the prey at random
  For I = 1:N
      Phase 1: Moving towards prey (exploration phase)
    For j = 1:m
      Calculate new status of the jth dimension using Equation (36)
    End
    Update the ith population member using Equation (37)
    Phase 2: Winging on the water surface (exploitation phase)
      For j = 1: m
        Calculate new status of the jth dimension using Equation (38)
      End
      Update the ith population member using Equation (39)
    End
    Update best candidate solution
End
Output best candidate solution obtained by POA
```

Figure 9. Pseudocode POA technique.

4. Results and Discussions

4.1. Comparing the Performance of Different Optimization Techniques

The study compared the performance of the proposed POA-PID with different optimization techniques, PSO-PID, MFOA-PID, HHO-PID, and GWO-PID, in a power system with a 1% load disturbance to explore the superiority of the proposed approach. The system's response was examined to determine its efficacy. Figure 10 illustrates the convergence behavior of the POA technique and different optimization algorithm techniques, showing how they progress towards optimal parameters over successive iterations. The convergence curve shows the efficiency of the optimization process, with a steeper decline indicating a faster approach towards the optimum fitness value. The graph shows the speed and stability of convergence, indicating the algorithms' potential to fine-tune controller parameters to mitigate system frequency deviations following load changes. Figure 10 demonstrates that the POA technique exhibits faster convergence (8^{th} iteration-red circle) and lower frequency deviations (0.001687 Hz), indicating greater reliability and efficiency compared to GWO, PSO, MFOA, and HHO.

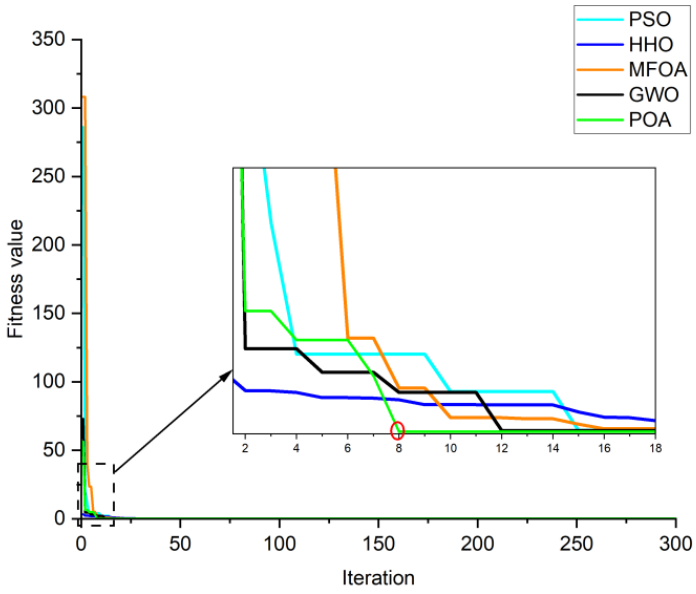


Figure 10. PSO, HHO, MFOA, GWO, and POA convergence characteristics.

The graphical data in Figure 11 show frequency deviation responses for a four-area power network, each tuned with a different optimization algorithm. Area 1 (Figure 11a) shows the POA with a rapid initial response and quick stabilization, while PSO and GWO show a slightly delayed response with more pronounced oscillations. HHO and MFOA responses are similar to POA, but HHO exhibits a slightly slower convergence to a steady state. Area 2 (Figure 11b) shows the POA with a swift response, minimal overshoot, and a stable steady state. PSO and MFOA display more significant overshoots and longer settling times, with PSO showing the most important deviation before recovery. HHO and GWO are closer to POA's performance, with GWO showing a rapid initial response but more oscillatory behavior. Area 3 (Figure 11c) shows the POA with a stable response, while PSO and HHO show large deviations and oscillations. MFOA's response is aggressive, with the most significant initial overshoot, but it settles relatively quickly. Area 4 (Figure 11d) shows the POA's performance with the lowest overshoot and quickest stabilization, while PSO exhibits significant undershoot and a slow return to stability.

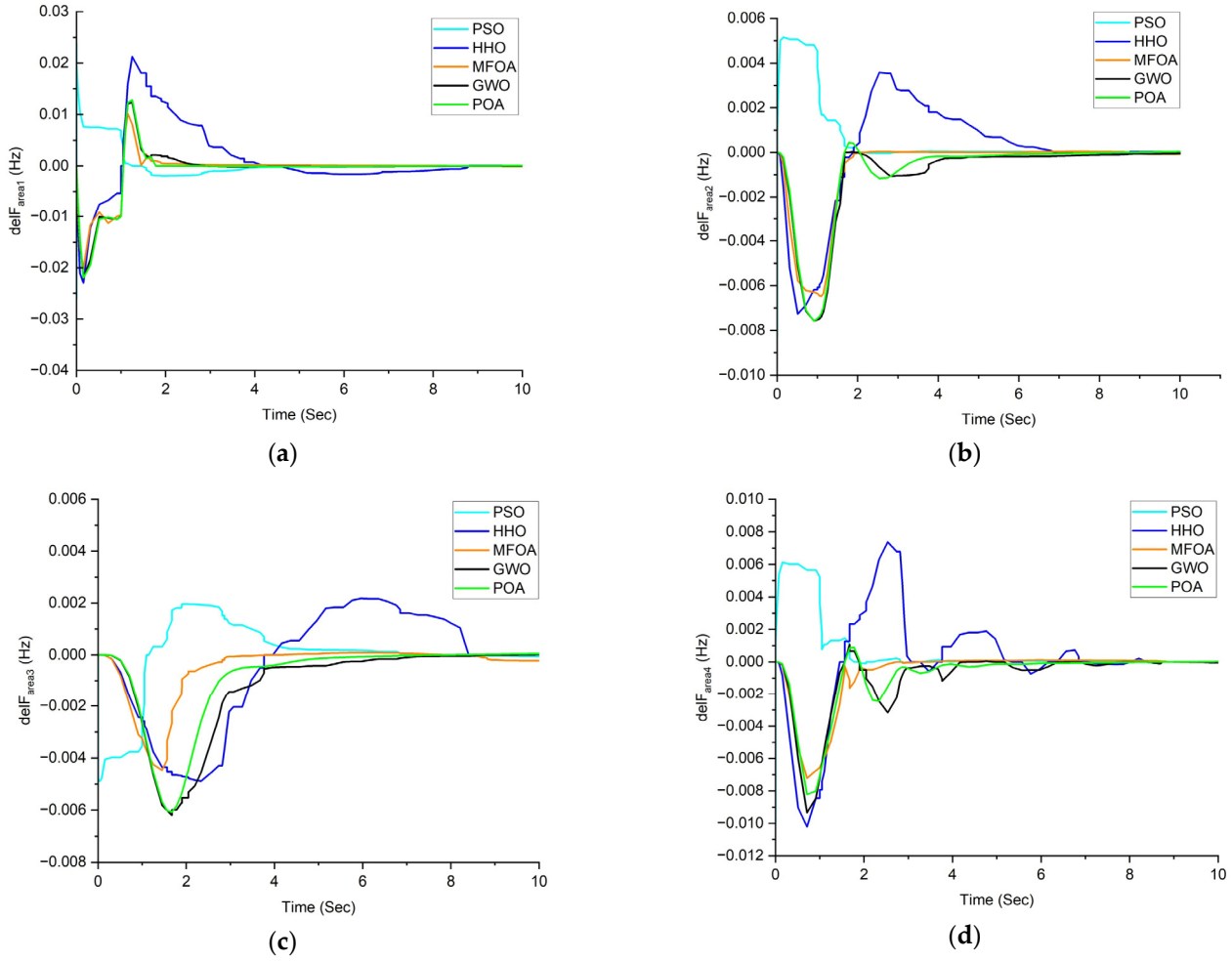


Figure 11. Frequency deviation for (**a**) Area 1, (**b**) Area 2, (**c**) Area 3, and (**d**) Area 4.

Figure 12 illustrates the tie-line power flow deviations between different areas of a four-area power network controlled by various optimization algorithms. The POA method significantly reduces power flow deviation in Figure 12a, the tie-line between Areas 1 and 2, with minimal overshoot and a quick settling time to a steady state. This is compared to PSO, GWO, MFOA, and HHO, which show more significant initial deviations and longer settling times. HHO, in particular, shows a slower approach to steady state, suggesting a less optimal response. In Figure 12b, the tie-line between Areas 2 and 3 is stable with minimal deviation and the fastest return to stability, while PSO shows significant deviation

and a prolonged settling period. In Figure 12c, the tie-line between Areas 3 and 4 is effective, with minimal overshoot. The GWO method responds quickly but has a more significant overshoot. PSO and HHO show the most deviations and fail to settle within a 10 s timeframe, suggesting a less effective control strategy. Figure 12d shows tie-line power flow deviation between Areas 1 and 4, with minimal overshoot. MFOA and GWO show similar initial responses but with more oscillation before stabilization. PSO and HHO show more significant initial deviations, with PSO struggling to stabilize.

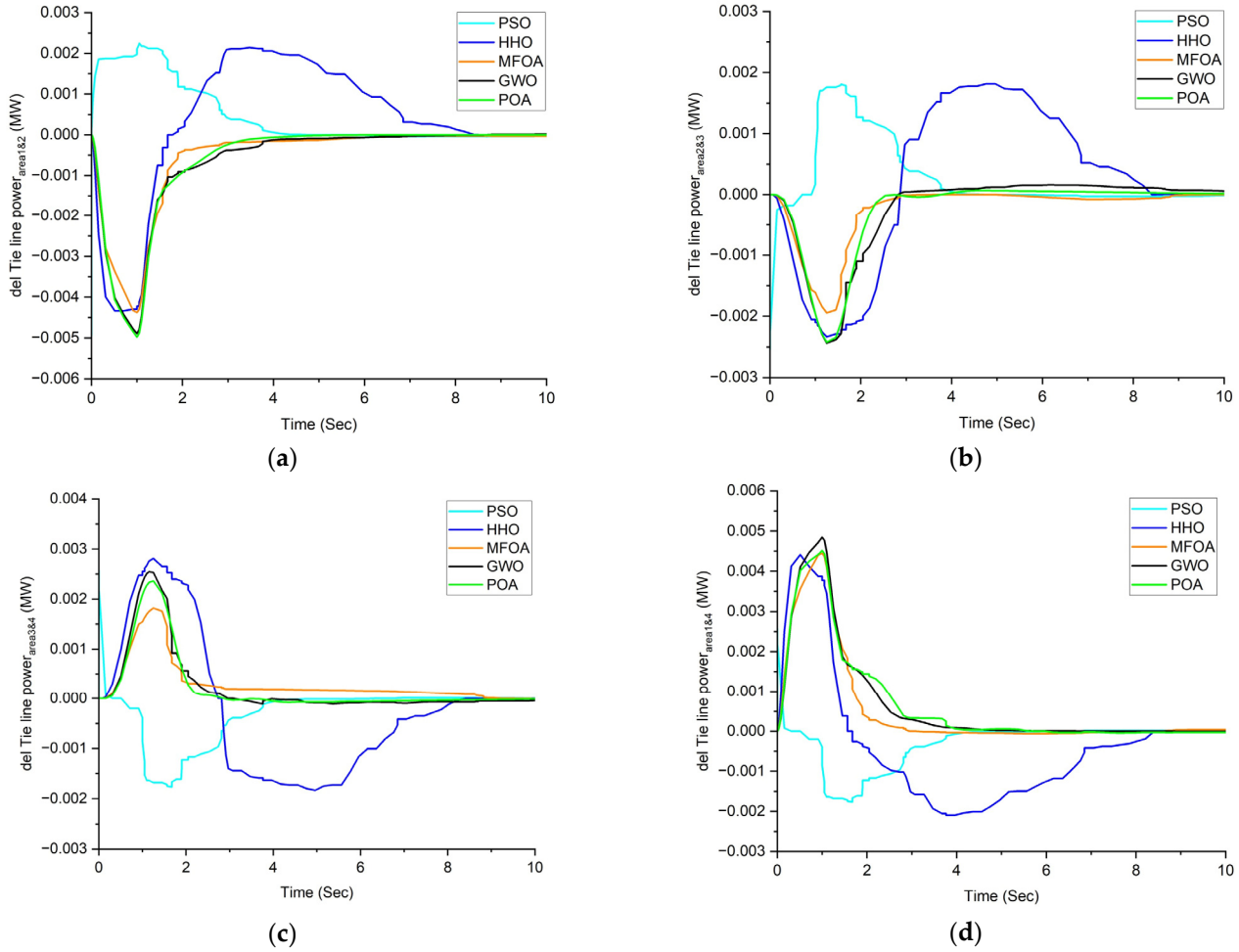


Figure 12. Tie-line power flow deviation for (**a**) Areas 1 and 2, (**b**) Areas 2 and 3, (**c**) Areas 3 and 4, and (**d**) Areas 1 and 4.

Figures 13 and 14 visually represent the comparison, presenting bar charts to explain the differences in settling times across all areas and tie-lines. Figure 13 shows that the POA-PID controller significantly reduces settling times in system frequency compared to the GWO, PSO, MFOA, and HHO-PID-PID across all areas. In Area 1, the POA-PID controller reduced response times by an average of 55.27%. In contrast, in Area 2, the POA-PID controller surpassed the GWO and HHO controller's response time by an average of 28.6%, although it was 1 s slower than both PSO and MFOA controllers. In Area 3, it improved by an average of 42.21%, and in Area 4, it reduced response times from GWO and HHO controllers by an average of 40.97%, while it was 1 s slower than both PSO and MFOA controllers. These response times reflect the control system's agility and efficiency in maintaining power system frequency stability. The POA technique is more adept at optimizing PID controller parameters, resulting in a more responsive and robust power network. The superiority is particularly pronounced in Area 1, where the response time is

more than halved, underscoring the POA's potential to enhance the dynamic performance of load frequency control systems.

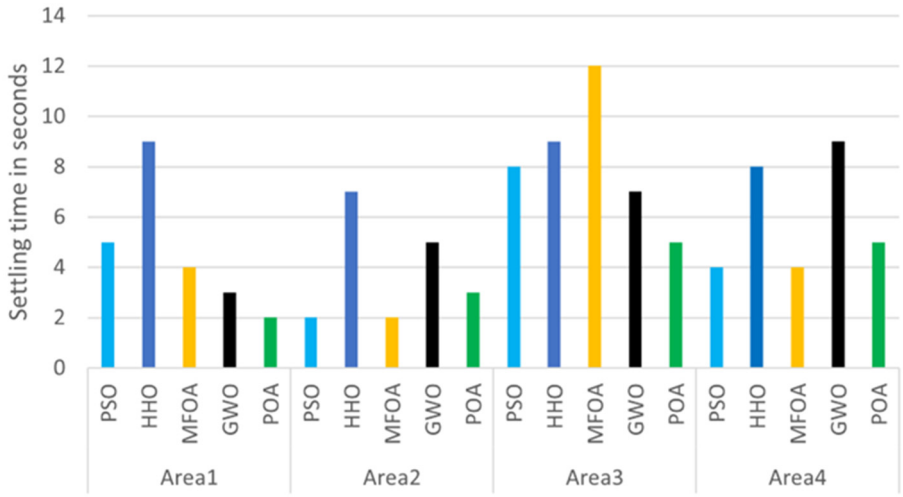


Figure 13. Comparison of settling time in system frequency.

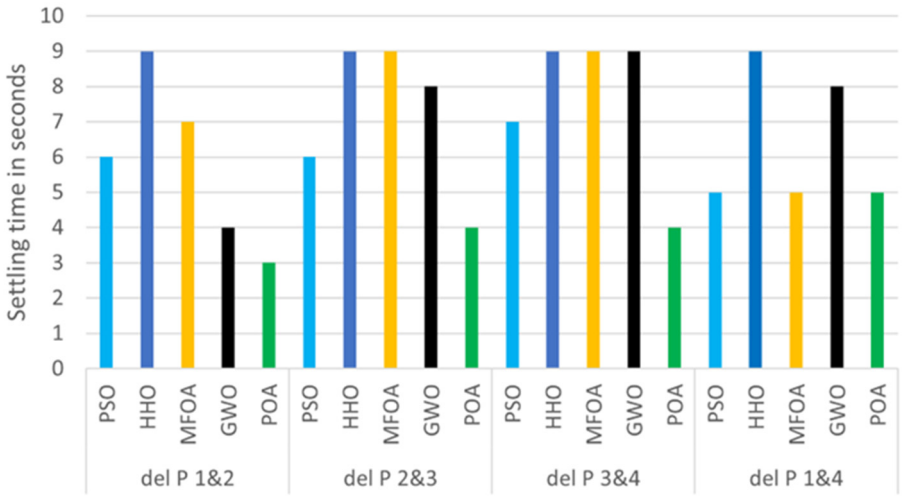


Figure 14. Comparison of settling time in tie-line power flow.

The POA-PID controller effectively manages tie-line power flows, demonstrating faster settling times than the GWO, PSO, MFOA, and HHO-PID controllers. In Figure 14, for the case of tie-line perturbations ($delP_{1,2}$; $delP_{2,3}$; $delP_{3,4}$; $delP_{1,4}$), $delP_{1,2}$ scenario, the POA-PID controller settles oscillations in 3 s with significantly faster response times than by an average of 49.70%. In $delP_{2,3}$ and $delP_{3,4}$ scenarios, the POA-PID controller outperforms by settling oscillations in 4 s. Even in the challenging $delP_{1,4}$ scenario, the POA-PID controller quickly responds by settling in 5 s, demonstrating dominance over the GWO and HHO-PID. The comprehensive analysis of the response behavior of the POA-PID controller, especially when benchmarked against the GWO, PSO, HHO, and MFOA controllers, highlights the advantages of the POA in tuning PID controllers for power systems with diverse sources like thermal, hydro, and gas. The POA-PID controller enhances system resilience to load disturbances and improves the operational efficiency of LFC.

The comparison of improved controller gain values in Table 1 involves examining each parameter of the PID controller across four areas and how they are optimized by different algorithms: PSO, HHO, MFOA, GWO, and the proposed POA. The proportional gain (K_p)

values for Areas 1 and 2 are set or converged to 10, suggesting a possible constraint or common starting point in the optimization process. However, for Areas 3 and 4, POA presents a distinctly lower proportional gain, especially in Area 4, with a K_p of 6.926 compared to other algorithms. The integral gain (K_i) values show significant differences. POA suggests a moderately higher (K_i) value in Area 1 but much lower than HHO, indicating a balance between rapid error correction and system stability. POA's approach for (K_D) values shows conservative tuning in Area 1 and more aggressive tuning in Areas 2 and 3, with values leaning towards quicker responses to changes in system error rates.

Table 1. Improved PID controller gain values for different optimization techniques.

Optimization Methods	Area 1			Area 2			Area 3			Area 4		
	K_{P-1}	K_{I-1}	K_{D-1}	K_{P-2}	K_{I-2}	K_{D-2}	K_{P-3}	K_{I-3}	K_{D-3}	K_{P-4}	K_{I-4}	K_{D-4}
PSO	10	7.399	5.882	10	−2.760	10	−4.275	0.531	−1.141	−3.688	0.327	10
HHO	10	8.329	7.238	5.768	8.069	8.927	−3.893	0.402	−0.892	8.650	5.704	8.349
MFOA	10	−0.060	9.983	9.998	10	10	−10	1.394	−6.341	−1.405	0.996	8.437
GWO	10	7.872	5.685	−1.720	0.108	0.719	−8.660	−0.033	−0.649	2.612	0.037	10
POA	10	0.046	8.049	8.553	4.583	5.842	−9.046	−0.017	−0.041	6.926	0.892	9.974

In Table 2, the ITAE values serve as a performance metric for each optimized PID controller. The POA-PID controller demonstrates superior performance with the lowest ITAE value of 0.084346, indicating more accurate and faster settling of frequency deviations post-load perturbation. MFOA-PID and GWO-PID exhibit competitive performance with ITAE values of 0.091004 and 0.090714, closely following POA-PID. HHO-PID, while better than PSO-PID, still lags behind the proposed POA-PID with an ITAE of 0.170664.

Table 2. Values of ITAE for different optimization techniques.

Controller	ITAE
PSO-PID	0.156113
MFOA-PID	0.091004
HHO-PID	0.170664
GWO-PID	0.090714
Proposed POA-PID	0.084346

Overall, the POA-PID algorithm outperforms the PSO and HHO algorithms by over 45.97% and 50.57%, respectively. The ITAE values for MFOA-PID and GWO-PID are 7.31% and 7.01% higher than the POA-PID. The POA-PID controller's tuning results in the best performance, with the lowest ITAE value, indicating a more optimal balance between responsiveness and stability in the LFC system. The POA approach enhances the system's dynamic response compared to conventional optimization techniques, highlighting its potential in optimizing control systems for interconnected four-area power systems.

4.2. Robustness Analysis

The proposed POA-PID controller performance is verified by the following two scenarios A and B. Scenario A performed a sensitivity analysis of this system by variations of ±25% and ±50% in the following speed regulation (R), tie-line coefficient (T_{ij}), and power system time constant (T_p) from the nominal values, and scenario B comprises variations in load disturbance.

4.2.1. Scenario A: Sensitivity Analysis

The study examines the sensitivity of the power system's response to parameters such as speed regulation (R), tie-line coefficient (T_{ij}), and power system time constant (T_p). The parameters were varied by ±25% and ±50% from their nominal values to assess

the robustness of the POA-PID controller in the proposed power system framework. The analysis was designed to gauge the system's resilience to a standardized load perturbation (SLP) set at 1%. Table 3 shows that a 50% increase in R led to slight variations in frequency deviations, indicating a tolerable resilience to parameter increases. A 25% increase showed similar trends with marginally better frequency stability than the 50% increase. A decrease in R by 25% and 50% exhibited increased frequency deviations, signaling a need to adjust control strategies for lower R-values. The increased values of T_{ij} demonstrated the system's capacity to absorb changes without significant degradation in performance. The decreased values of T_p showed a quicker response but at the expense of more significant deviations, which might demand faster but more nuanced control reactions. The sensitivity analysis in scenario A revealed that while the POA-PID controller is robust, it has varying degrees of sensitivity to parameter changes. This scenario's improved frequency stability specification parameters are shown in Figure 15a, i.e., 25% and 50% decreases in R lead to increased frequency deviations, while the system's ability in Figure 15b T_{ij} to absorb changes without significant performance degradation is demonstrated. However, in Figure 15c, the decreased values of T_p result in quicker responses but more significant deviations.

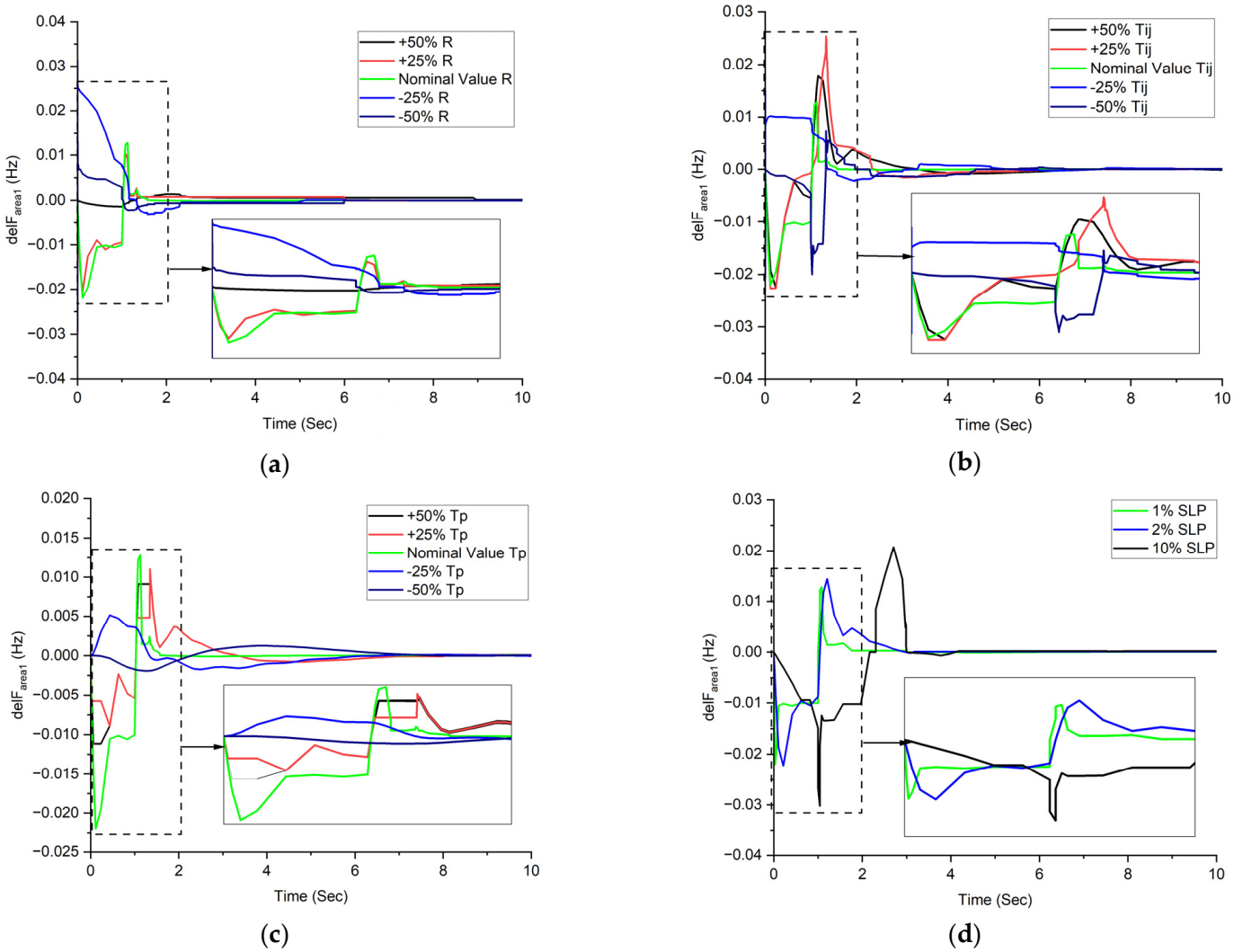


Figure 15. Frequency deviation in Area 1 for 1% SLP and variations (**a**) speed regulator; (**b**) tie-line coefficient; (**c**) time constant for ±25% and ±50%; and (**d**) in Area 1 for 1%, 2%, and 10% SLP.

Table 3. Optimized frequency stability specification parameters of the POA-PID controller.

Parameters	T_s(s)				OS (Hz) (10^{-3})				US (Hz) (10^{-3})			
	Δf_1	Δf_2	Δf_3	Δf_4	Δf_1	Δf_2	Δf_3	Δf_4	Δf_1	Δf_2	Δf_3	Δf_4
+50% R	9	10	7	8	1.6	0	0.0785	0.056	1	0.215	0.19	0.2265
+25% R	6	7	7	8	0.5	0	0	0.005	0.85	0.25	0.115	0.39
Nominal R-value	2	3	5	5	0.65	0.0475	0	0.05	1.15	0.375	0.3	0.4
−25% R	5	5	6	5	1.4	0.225	0.15	0.45	1.25	0.35	0.4	0.5
−50% R	6	7	6	7	1.65	0.36	0.09045	0.465	1.45	0.5425	0.25	0.55
+50% T_{ij}	8	9	8	11	0.89	0.045	0	0.136	1.1	0.185	0.19	0.485
+25% T_{ij}	7	6	6	9	1.05	0.0262	0.121	0.4	1.13	0.215	0.26	0.51
Nominal T_{ij} value	2	3	5	5	0.65	0.0475	0	0.05	1.15	0.375	0.3	0.4
−25% T_{ij}	8	7	9	8	0.75	0.128	0.307	0.307	1	0.315	0.33	0.315
−50% T_{ij}	8	9	9	10	0.37	0.006	0.073	0.001	1	0.25	0.355	0.232
+50% T_p	8	10	9	8	0.50	0.050	0.250	0.115	0.60	0.245	0.175	0.575
+25% T_p	8	7	9	10	0.57	0.025	0	0.35	0.45	0.340	0.10	0.450
Nominal T_p value	2	3	5	5	0.65	0.0475	0	0.05	1.15	0.375	0.3	0.4
−25% T_p	9	6	7	10	0.25	0.160	0.1	0.275	0.14	0.270	0.275	0.650
−50% T_p	8	11	9	7	0.075	0.01	0.045	0.05	0.1	0.150	0.385	0.345

4.2.2. Scenario B: Load Disturbance Analysis

Scenario B of the study assessed the performance of a system under different load disturbances, specifically 1%, 2%, and 10% in Area 1 of the network. The system's performance was evaluated under these conditions, demonstrating its ability to handle unexpected changes in load. At 1% SLP load disturbance, the system showed transient behavior with a settling time of 2 s, with moderately low overshoot and undershoot. When the disturbance increased to 2%, the system experienced a higher overshoot and a settling time of 3 s. However, the system stabilized within an acceptable timeframe, demonstrating its effective damping. At 10% SLP load disturbance, the system experienced a significant disturbance of 10%, with a settling time of 4 s, an overshoot of 1 Hz, and an undershoot of 1.5 Hz. Despite these deviations, the system successfully returned to a stable state without prolonged oscillations, demonstrating its capacity to manage severe disturbances in the settling time (TS), overshoot (OS), and undershoot (US) parameters of the robustness test from Figure 15d. According to the findings in Table 4, the system stability and reliability of the POA technique clearly show the proposed POA-PID controller gives superior performance during different load conditions.

Table 4. TS, OS, and US of frequency deviation Area 1 for load disturbance analysis.

Load Disturbance	T_S	OS (Hz)	US (Hz)
1% SLP	2	0.65	1.15
2% SLP	3	0.75	1.17
10% SLP	4	1	1.5

According to the findings of scenarios A and B, the proposed POA-PID controller effectively functioned despite load variations, maintaining performance parameters with remarkable resilience. Even under severe disturbances, the maximum deviation in settling time did not exceed 11 s, demonstrating the control strategy's effectiveness in maintaining system frequency stability.

4.3. Comparative Analysis

Results obtained through the optimization of the PID controller using various optimization techniques for stabilizing load frequency in power systems are compared with that of the proposed POA in Table 5. The POA-PID in reheat thermal systems shows substantial frequency deviations (Δf_1, Δf_2, Δf_3, Δf_4) with high ITAE values. However, the

BSA-PID in hydro–thermal systems reduces these deviations and achieves a lower ITAE. The GSA-PID reduces frequency deviation across multi-area hydro systems, but the ITAE has not been reported. The GA-PID and PSO-PID in two-area systems involving hydro, thermal, and gas sources result in higher frequency deviations, suggesting less optimal performance. The MFOA achieves the lowest deviations in two-area thermal systems but does not improve upon the ITAE. The HHO-PID in renewable energy systems and the GWO-PID in diverse power systems present higher deviations, especially in Δf_2 and Δf_3, indicating slower response in multi-area settings. The proposed POA-PID in a complex four-area system shows the most minor frequency deviations and lowest ITAE value compared to WCA [24], BSA [28], and MFOA [32] optimization techniques. Table 6 shows enhanced efficiency by margins of 36.99%, 27.82%, and 34.54%, respectively.

Table 5. Comparative analysis of LFC in multi-area power systems.

Ref.	Power Systems	Techniques	T_s (s)				ITAE
			Δf_1	Δf_2	Δf_3	Δf_4	
[24]	Reheat Thermal, Hydro (Four Areas)	WCA-PID	9.55	12.52	12.54	27.41	0.1338
[28]	Hydro–Thermal (Four Areas)	BSA-PID	4.5	4	3.33	3.2	0.1168
[29]	Thermal, Hydro, Hydro, Hydro (Four Areas)	GSA-PID	5.96	5.30	8.69	7.88	-
[30]	Hydro, Thermal, Gas (Two Areas)	GA-PID	14.54	15.22	-	-	-
[31]	Hydro, Thermal, Gas (Two Areas)	PSO-PID	14.54	15.22	-	-	-
[32]	Thermal Systems (Two-Area)	MFOA-PID	2.59	3.71	-	-	0.1288
[33]	Wind, Solar, Tidal (Three Areas)	HHO-PID	6.24	13.77	14.02	-	-
[34]	Thermal, Nuclear, Hydro (Three Areas)	GWO-PID	14	17	17	-	-
Proposed work	Non-Reheat thermal, Thermal with Reheat, Hydro, Gas (Four Areas)	POA-PID	2	3	5	5	0.0843

Table 6. Comparison of optimization techniques in power systems gain ITAE value.

Optimization Techniques	ITAE Improvement of POA over Other Techniques
GWO	7.01%
MFOA	7.31%
PSO	45.97%
HHO	50.57%
WCA-PID [24]	36.99%
BSA-PID [28]	27.82%
MFOA-PID [32]	34.54%

5. Conclusions

This study introduces an LFC mechanism for an ith area interconnected power network using a PID controller enhanced through the POA. The POA technique is utilized to optimize the gain parameters of the PID controller, ensuring the system output power is maintained without damping oscillations during unpredicted load-varying conditions in the tie-line between interconnected areas. The proposed POA-PID controller significantly improves control efficacy in a complex, four-area power grid, reducing the ITAE value to 0.084346. Compared to conventional optimization techniques, GWO, MFOA, PSO, and HHO, the POA-PID controller shows enhanced efficiency by margins of 7.01%, 7.31%, 45.97%, and 50.57%, respectively, in a diverse-generation unit power network. This underscores the robust optimization capability of the POA, setting new benchmarks for load frequency and tie-line power flow control efficiency by an average of 45.56% and 42.79%, respectively. The POA-PID controller demonstrated

remarkable resilience despite load variations, maintaining performance parameters and system frequency stability, with a maximum deviation of 11 s under severe disturbances.

The findings highlight the efficacy of the POA-PID controller in managing interconnected power systems. The POA addresses key technical challenges, including managing dynamic load changes, handling the complexities of multi-area systems, and minimizing frequency deviations. It provides adaptive tuning of PID controller parameters, enhancing system responsiveness to sudden load variations and achieving quicker stabilization and improved overall stability but acknowledges limitations such as implementing the POA requires substantial computational resources and expertise. Its scalability in larger systems needs further testing, and real-time optimization presents challenges demanding advanced computational capabilities. Ensuring consistent performance across diverse scenarios and integrating POA with existing infrastructure may require system modifications.

Future work aims to extend the applicability and robustness of the POA-based PID controller by testing in a broader array of power system configurations, incorporating a more comprehensive range of load disturbances, developing hybrid optimization techniques, and implementing the controller in more realistic environments.

Author Contributions: Conceptualization, A.R.S., M.A.T. and S.A.; methodology, M.A.T., A.R.S. and S.A.; software, A.R.S. and M.A.T.; validation, S.A., G.M.S., M.R.H., M.R.A. and T.A.; formal analysis, M.R.H., M.R.A. and T.A.; investigation, S.A., A.R.S., M.A.T. and M.R.H.; funding acquisition, G.M.S. and S.A.; data curation, S.A., M.A.T. and A.R.S.; writing—original draft preparation, M.A.T., A.R.S. and S.A.; writing—review and editing, G.M.S., T.A., M.R.A. and M.R.H.; visualization, A.R.S. and M.A.T.; supervision, S.A., T.A. and M.R.A. All authors have read and agreed to the published version of the manuscript.

Funding: The authors would like to thank American International University–Bangladesh (AIUB) for providing financial support under the AIUB Research Grant # AIUB-FE-24-02-01.

Data Availability Statement: Data can be found within this study.

Acknowledgments: The authors would like to thank the American International University–Bangladesh (AIUB) and Murdoch University, Australia, for providing all kinds of research support to complete the research.

Conflicts of Interest: The authors declare no conflicts of interest.

Abbreviations

Symbols	Description	Symbols	Description
ΔX_{Gi}	Deviation in governor valve position (p.u.MW)	T_{SG}	Constant time of speed governor (s)
ΔP_{Ci}	Deviation in output of controller (p.u.MW)	T_t	Constant time of turbine (s)
ΔP_{Gi}	Deviation in mechanical output (p.u.MW)	T_r	Reheat time constant (s)
ΔP_{Li}	Deviation load disturbance (p.u.MW)	K_r	Reheat gain (Hz/p.u.MW)
ΔP_{Li}	Tie-line power flow (p.u.MW)	T_{SG}	Constant time of speed governor (s)
Δf_i	Deviation in frequency (Hz)	X_g	Time constant of governor lead (s)
ΔE_i	Deviation in integral control (p.u.MW)	T_{gh}	Time constant for hydropower plant (s)
T_{Gi}	Governor time constant (sec.)	T_{rh}	Time constant for drop compensation (s)
T_{ti}	Constant time of governor (sec.)	B_g	Positioner constant for gas turbine (s)
T_{Pi}	Constant time of power system and machine (sec.)	C_g	Valve constant for gas turbine (s)
T_{ij}	Interconnection tie-line gain (p.u.MW/rad/s.) between areas i and j	T_W	Water stating/penstock turbine constant time (s)
K_{Pi}	Power system and machine gain (Hz/p.u.MW)	Y_g	Time constant of governor lag (s)
R_i	Speed regulation coefficient (Hz/p.u.MW)	T_F	Time constant for fuel (s)
ACE	Area control error	T_{CR}	Time delay for combustion reaction (s)
β_i	Frequency bias factor (p.u.MW/Hz)	T_{CD}	Time constant for combustion discharge volume (s)
E	Terminal voltage	δ	Angle of the voltage E
$\Delta\delta$	Change in angle	X_{ij}	Interconnection reactance between areas i and j
$P_{tie,\ ij}$	Tie-line power flow between areas i and j	P_{ri}	Rated capacity of each area
a_{ij}	Coefficient between areas i and j	H	Inertia constant (MW-s/MVA)
D	Load frequency characteristics (p.u.MW/Hz)	$\Delta\omega_i$	Deviation in area frequency (Hz)

Appendix A

Table A1. Parameters of the four-area interconnected power system.

Symbol	Parameter
f	60 Hz
$R_1 = R_2 = R_3 = R_4$	2.4 Hz/p.u.MW
$P_{r1} = P_{r2} = P_{r3} = P_{r4}$	2000 MW
ΔP_L	0.01
B	0.545 p.u.MW/Hz
T_G (Thermal)	0.08 s
T_t	0.3 s
K_P	120 Hz.p.u./MW
T_P	20 s
T_r	10 s
K_r	0.5
T_G (Hydro)	0.2 s
T_g	4.9 s
T_G (Gas)	28.749 s
T_W	1.1 s
X_G	0.6 s
Y_G	1.1 s
B_G	0.049 s
C_G	1 s
T_{cr}	0.01 s
T_F	0.239 s
T_{CD}	0.2 s
$2\pi T_{12} = 2\pi T_{23} = 2\pi T_{34} = 2\pi T_{41}$	0.545

References

1. Veloza, O.P.; Santamaria, F. Analysis of Major Blackouts from 2003 to 2015: Classification of Incidents and Review of Main Causes. *Electr. J.* **2016**, *29*, 42–49. [CrossRef]
2. Liu, Z.; Zhang, Y.; Wang, Y.; Wei, N.; Gu, C. Development of the Interconnected Power Grid in Europe and Suggestions for the Energy Internet in China. *Glob. Energy Interconnect.* **2020**, *3*, 111–119. [CrossRef]
3. Ram Babu, N.; Bhagat, S.K.; Saikia, L.C.; Chiranjeevi, T.; Devarapalli, R.; García Márquez, F.P. A Comprehensive Review of Recent Strategies on Automatic Generation Control/Load Frequency Control in Power Systems. *Arch. Comput. Methods Eng.* **2023**, *30*, 543–572. [CrossRef]
4. Prabasa, R.; Arsyad, M.I.; Pontia, W.F.T. Study of Electrical Installation Planning at the General Hospital in Bengkayang District. *Telecommun. Comput. Electr. Eng. J.* **2023**, *1*, 1–12. [CrossRef]
5. Wang, W.; Yin, H.; Chen, C.; Till, A.; Yao, W.; Deng, X.; Liu, Y. Frequency Disturbance Event Detection Based on Synchrophasors and Deep Learning. *IEEE Trans. Smart Grid* **2020**, *11*, 3593–3605. [CrossRef]
6. Kumar, L.V.S.; Ananth, D.V.N.; Kumar, Y.V.P.; Pradeep, D.J.; Reddy, C.P.; Ariwa, E. Use of Super Conductor Magnetic Energy Storage System and FACTS Devices for Two-Area Load Frequency Control Having Synchronous Generators and DFIG Wind Generators. *Int. J. Comput. Digit. Syst.* **2021**, *10*, 1227–1238. [CrossRef]
7. Zhang, Y.; Yang, T. Decentralized Switching Control Strategy for Load Frequency Control in Multi-Area Power Systems with Time Delay and Packet Losses. *IEEE Access* **2020**, *8*, 15838–15850. [CrossRef]
8. Ferdous, S.M.; Shahnia, F.; Shafiullah, G.M. Stability and Robustness of a Coupled Microgrid Cluster Formed by Various Coupling Structures. *Chin. J. Electr. Eng.* **2021**, *7*, 60–77. [CrossRef]
9. Aziz, A.; Shafiullah, G.M.; Stojcevski, A.; Mto, A. Participation of DFIG Based Wind Energy System in Load Frequency Control of Interconnected Multigeneration Power System. In Proceedings of the 2014 Australasian Universities Power Engineering Conference (AUPEC), Perth, WA, Australia, 28 September–1 October 2014.
10. Ferdous, S.M.; Shafiullah, G.M.; Shahnia, F.; Elavarasan, R.M.; Subramaniam, U. Dynamic Frequency and Overload Management in Autonomous Coupled Microgrids for Self-Healing and Resiliency Improvement. *IEEE Access* **2020**, *8*, 116796–116811. [CrossRef]
11. Mishra, S.; Prusty, U.C.; Prusty, R.C.; Panda, S. Novel Load Frequency Control Scheme for Hybrid Power Systems Employing Interline Power Flow Controller and Redox Flow Battery. *Energy Sources Recovery Util. Environ. Eff.* **2021**, 1–19. [CrossRef]
12. Rumky, T.J.; Ahmed, T.; Ahmed, M.; Mekhilef, S. Tri-Band Damping Controller for Low Frequency Oscillations in AC Microgrid System. In Proceedings of the 2023 IEEE IAS Global Conference on Renewable Energy and Hydrogen Technologies (GlobConHT), Male, Maldives, 11–12 March 2023.

13. Ahmad, S.; Awalin, L.J.; Ferdous Riya, J.; Billah, A.M.; Ahmed, T.; Mekhilef, S.; Mokhlis, H.; Seyedmahmoudian, M.; Stojcevski, A. Smart Interconnection Method for Integrating Two Microgrids. In Proceedings of the 2023 33rd Australasian Universities Power Engineering Conference (AUPEC), Ballarat, Australia, 25–27 September 2023.
14. Ahmed, T.; Mekhilef, S.; Shah, R.; Mithulananthan, N. Investigation into Transmission Options for Cross-Border Power Trading in ASEAN Power Grid. *Energy Policy* **2017**, *108*, 91–101. [CrossRef]
15. Mohamed, M.A.E.; Jagatheesan, K.; Anand, B. Modern PID/FOPID Controllers for Frequency Regulation of Interconnected Power System by Considering Different Cost Functions. *Sci. Rep.* **2023**, *13*, 14084. [CrossRef]
16. Barakat, M. Optimal Design of Fuzzy-PID Controller for Automatic Generation Control of Multi-Source Interconnected Power System. *Neural Comput. Appl.* **2022**, *34*, 18859–18880. [CrossRef]
17. Yan, Z.; Xu, Y. A Multi-Agent Deep Reinforcement Learning Method for Cooperative Load Frequency Control of a Multi-Area Power System. *IEEE Trans. Power Syst.* **2020**, *35*, 4599–4608. [CrossRef]
18. Liu, X.; Qiu, L.; Fang, Y.; Wang, K.; Li, Y.; Rodríguez, J. Finite Control-Set Learning Predictive Control for Power Converters. *IEEE Trans. Ind. Electron.* **2024**, *71*, 8190–8196. [CrossRef]
19. Liu, X.; Qiu, L.; Fang, Y.; Wang, K.; Li, Y.; Rodríguez, J. Predictive Control of Voltage Source Inverter: An Online Reinforcement Learning Solution. *IEEE Trans. Ind. Electron.* **2024**, *71*, 6591–6600. [CrossRef]
20. Entezari, A.; Bahari, M.; Aslani, A.; Ghahremani, S.; Pourfayaz, F. Systematic Analysis and Multi-Objective Optimization of Integrated Power Generation Cycle for a Thermal Power Plant Using Genetic Algorithm. *Energy Convers. Manag.* **2021**, *241*, 114309. [CrossRef]
21. Onyeka, A.E.; Xing-Gang, Y.; Mao, Z.; Jiang, B.; Zhang, Q. Robust Decentralised Load Frequency Control for Interconnected Time Delay Power Systems Using Sliding Mode Techniques. *IET Control Theory Appl.* **2020**, *14*, 470–480. [CrossRef]
22. Weldcherkos, T.; Salau, A.O.; Ashagrie, A. Modeling and Design of an Automatic Generation Control for Hydropower Plants Using Neuro-Fuzzy Controller. *Energy Rep.* **2021**, *7*, 6626–6637. [CrossRef]
23. Kalyan, C.; Goud, B.; Reddy, C.; Ramadan, H.; Bajaj, M.; Ali, Z. Water Cycle Algorithm Optimized Type II Fuzzy Controller for Load Frequency Control of a Multi-Area, Multi-Fuel System with Communication Time Delays. *Energies* **2021**, *14*, 5387. [CrossRef]
24. Ullah, K.; Basit, A.; Ullah, Z.; Aslam, S.; Herodotou, H. Automatic Generation Control Strategies in Conventional and Modern Power Systems: A Comprehensive Overview. *Energies* **2021**, *14*, 2376. [CrossRef]
25. Sun, Y. PID Controller Combined with Intelligent Algorithm. *Appl. Comput. Eng.* **2023**, *6*, 490–496. [CrossRef]
26. Lee, D.; Koo, S.; Jang, I.; Kim, J. Comparison of Deep Reinforcement Learning and PID Controllers for Automatic Cold Shutdown Operation. *Energies* **2022**, *15*, 2834. [CrossRef]
27. Razali, M.R.; Mohd Faudzi, A.A.; Shamsudin, A.U.; Mohamaddan, S. A Hybrid Controller Method with Genetic Algorithm Optimization to Measure Position and Angular for Mobile Robot Motion Control. *Front. Robot. AI* **2023**, *9*, 1087371. [CrossRef]
28. Khadanga, R.K.; Kumar, A.; Panda, S. A Novel Sine Augmented Scaled Sine Cosine Algorithm for Frequency Control Issues of a Hybrid Distributed Two-Area Power System. *Neural Comput. Appl.* **2021**, *33*, 12791–12804. [CrossRef]
29. Ali, T.; Malik, S.A.; Hameed, I.A.; Daraz, A.; Mujlid, H.; Azar, A.T. Load Frequency Control and Automatic Voltage Regulation in a Multi-Area Interconnected Power System Using Nature-Inspired Computation-Based Control Methodology. *Sustainability* **2022**, *14*, 12162. [CrossRef]
30. Guha, D.; Roy, P.K.; Banerjee, S. A Maiden Application of Modified Grey Wolf Algorithm Optimized Cascade Tilt-Integral-Derivative Controller in Load Frequency Control. In Proceedings of the 2018 20th National Power Systems Conference (NPSC), Tiruchirappalli, India, 14–16 December 2018.
31. Dogan, A. Load Frequency Control of Two Area and Multi Source Power System Using Grey Wolf Optimization Algorithm. In Proceedings of the 2019 11th International Conference on Electrical and Electronics Engineering (ELECO), Bursa, Turkey, 28–30 November 2019.
32. Debnath, M.K.; Jena, T.; Mallick, R.K. Novel PD-PID Cascaded Controller for Automatic Generation Control of a Multi-Area Interconnected Power System Optimized by Grey Wolf Optimization (GWO). In Proceedings of the 2016 IEEE 1st International Conference on Power Electronics, Intelligent Control and Energy Systems (ICPEICES), Delhi, India, 4–6 July 2016.
33. Guha, D.; Roy, P.K.; Banerjee, S. Load Frequency Control of Interconnected Power System Using Grey Wolf Optimization. *Swarm Evol. Comput.* **2016**, *27*, 97–115. [CrossRef]
34. Shakarami, M.R.; Faraji Davoudkhani, I. Wide-Area Power System Stabilizer Design Based on Grey Wolf Optimization Algorithm Considering the Time Delay. *Electr. Power Syst. Res.* **2016**, *133*, 149–159. [CrossRef]
35. Sahoo, B.P.; Panda, S. Improved Grey Wolf Optimization Technique for Fuzzy Aided PID Controller Design for Power System Frequency Control. *Sustain. Energy Grids Netw.* **2018**, *16*, 278–299. [CrossRef]
36. El-Hameed, M.A.; El-Fergany, A.A. Water Cycle Algorithm-based Load Frequency Controller for Interconnected Power Systems Comprising Non-linearity. *IET Gener. Transm. Distrib.* **2016**, *10*, 3950–3961. [CrossRef]
37. Guha, D.; Roy, P.K.; Banerjee, S. Application of Backtracking Search Algorithm in Load Frequency Control of Multi-Area Interconnected Power System. *Ain Shams Eng. J.* **2018**, *9*, 257–276. [CrossRef]
38. Yeboah, S.J. Gravitational Search Algorithm Based Automatic Load Frequency Control for Multi-Area Interconnected Power System. *Turk. J. Comput. Math. Educ. (TURCOMAT)* **2021**, *12*, 4548–4568.
39. Dhanasekaran, B.; Kaliannan, J.; Baskaran, A.; Dey, N.; Tavares, J.M.R.S. Load Frequency Control Assessment of a PSO-PID Controller for a Standalone Multi-Source Power System. *Technologies* **2023**, *11*, 22. [CrossRef]

40. Boopathi, D.; Jagatheesan, K.; Anand, B.; Samanta, S.; Dey, N. Frequency Regulation of Interlinked Microgrid System Using Mayfly Algorithm-Based PID Controller. *Sustainability* **2023**, *15*, 8829. [CrossRef]
41. Hakimuddin, N.; Khosla, A.; Garg, J.K. Comparative Performance Investigation of Genetic Algorithms (GAs), Particle Swarm Optimization (PSO) and Bacteria Foraging Algorithm (BFA) Based Automatic Generation Control (AGC) with Multi Source Power Plants (MSPPs). *Electr. Power Compon. Syst.* **2021**, *49*, 1513–1524. [CrossRef]
42. Mohanty, B. Performance Analysis of Moth Flame Optimization Algorithm for AGC System. *Int. J. Model. Simul.* **2019**, *39*, 73–87. [CrossRef]
43. Acharyulu, B.V.S.; Kumaraswamy, S.; Mohanty, B. Green Anaconda Optimized DRN Controller for Automatic Generation Control of Two-Area Interconnected Wind–Solar–Tidal System. *Electr. Eng.* **2023**, *1*, 1–6. [CrossRef]
44. Jagatheesan, K.; Boopathi, D.; Samanta, S.; Anand, B.; Dey, N. Grey Wolf Optimization Algorithm-Based PID Controller for Frequency Stabilization of Interconnected Power Generating System. *Soft Comput.* **2024**, *28*, 5057–5070. [CrossRef]
45. Yi, K.; Cai, C.; Tang, W.; Dai, X.; Wang, F.; Wen, F. A Rolling Bearing Fault Feature Extraction Algorithm Based on IPOA-VMD and MOMEDA. *Sensors* **2023**, *23*, 8620. [CrossRef]
46. Zhang, Y.; Li, H. Research on Economic Load Dispatch Problem of Microgrid Based on an Improved Pelican Optimization Algorithm. *Biomimetics* **2024**, *9*, 277. [CrossRef]
47. Husain, S.; Jarndal, A.; Hashmi, M.; Ghannouchi, F.M. Accurate, Efficient and Reliable Small-Signal Modeling Approaches for GaN HEMTs. *IEEE Access.* **2023**, *11*, 106833–106846. [CrossRef]
48. Ramakrishna, K.S.S.; Sharma, P.; Bhatti, T. Automatic Generation Control of Interconnected Power System with Diverse Sources of Power Generation. *Int. J. Eng. Sci. Technol. B Lagos* **2010**, *2*, 51–65. [CrossRef]
49. Prakash, S.; Sinha, S.K. Performance Evaluation of Hybrid Intelligent Controllers in Load Frequency Control of Multi Area Interconnected Power Systems. *Int. J. Electr. Comput. Eng.* **2013**, *2*, 515–524.
50. Kishor, N.; Saini, R.P.; Singh, S.P. A Review on Hydropower Plant Models and Control. *Renew. Sustain. Energy Rev.* **2007**, *11*, 776–796. [CrossRef]
51. Dhanasekaran, B.; Siddhan, S.; Kaliannan, J. Ant Colony Optimization Technique Tuned Controller for Frequency Regulation of Single Area Nuclear Power Generating System. *Microprocess. Microsyst.* **2020**, *73*, 102953. [CrossRef]
52. Trojovský, P.; Dehghani, M. Pelican Optimization Algorithm: A Novel Nature-Inspired Algorithm for Engineering Applications. *Sensors* **2022**, *22*, 855. [CrossRef]
53. Jagatheesan, K.; Anand, B.; Samanta, S.; Dey, N.; Santhi, V.; Ashour, A.S.; Balas, V.E. Application of Flower Pollination Algorithm in Load Frequency Control of Multi-Area Interconnected Power System with Nonlinearity. *Neural Comput. Appl.* **2017**, *28*, 475–488. [CrossRef]

Disclaimer/Publisher's Note: The statements, opinions and data contained in all publications are solely those of the individual author(s) and contributor(s) and not of MDPI and/or the editor(s). MDPI and/or the editor(s) disclaim responsibility for any injury to people or property resulting from any ideas, methods, instructions or products referred to in the content.